Structural and electronic transitions in $Ge_2Sb_2Te_5$ induced by ion irradiation damage

S. M. S. Privitera,[1] A. M. Mio,[1,*] E. Smecca,[1] A. Alberti,[1] W. Zhang,[2] R. Mazzarello,[3] J. Benke,[4] C. Persch,[4] F. La Via,[1] and E. Rimini[1,5]

[1]*Institute for Microelectronics and Microsystems (IMM), National Research Council (CNR), Zona Industriale, Ottava Strada 5, 95121, Catania, Italy*

[2]*Center for Advancing Materials Performance from the Nanoscale, State Key Laboratory for Mechanical Behavior of Materials, Xi'an Jiaotong University, Xi'an 710049, People's Republic of China*

[3]*Institute for Theoretical Solid State Physics, JARA-FIT and JARA-HPC, Rheinisch-Westfälische Technische Hochschule (RWTH) Aachen University, Aachen, Germany*

[4]*Physikalisches Institut (IA), RWTH Aachen University, Aachen, Germany*

[5]*Dipartimento di Fisica e Astronomia, Università di Catania, Catania, Italy*

(Received 10 June 2016; revised manuscript received 10 August 2016; published 6 September 2016)

$Ge_2Sb_2Te_5$ polycrystalline films either in the trigonal stable phase or in the metastable rock-salt structure have been irradiated with 150 keV Ar^+ ions. The effects of disorder are studied by electrical, optical, and structural measurements and density functional theory (DFT) simulations. In the metastable structure, the main effect of ion irradiation is a progressive amorphization, with an optical threshold at a fluence of 3×10^{13} cm^{-2}. For the trigonal structure, a metal-insulator transition and a crystalline transition to rock-salt structure occur prior to amorphization, which requires a fluence of 8×10^{13} cm^{-2}. The bonds of Te atoms close to the van der Waals gaps, present in the trigonal phase and identified by Raman spectroscopy, change as a function of the disorder induced by the irradiation. Comparison with DFT simulations shows that ion irradiation leads to the gradual filling of the van der Waals gaps with displaced Ge and Sb lattice atoms, giving rise first to a metal-insulator transition (9% of displaced atoms) correlated to the modification of the Te bonds and then induces a structural transition to the metastable rock-salt phase (15% of displaced atoms). The data presented here not only show the possibility to tune the degree of order, and therefore the electrical properties and the structure of phase change materials by ion irradiation, but also underline the importance of the van der Waals gaps in determining the transport mechanisms and the stability of the crystalline structure.

DOI: 10.1103/PhysRevB.94.094103

I. INTRODUCTION

Phase change materials, characterized by rapid switch between the amorphous and the crystalline phase, are among the most interesting candidates for replacing Flash memories for data storage applications [1–4]. Indeed, the two phases exhibit high contrast in the optical and electrical properties, and the phase change is induced by current pulses, with energy needs that depend on the material properties and on the device architecture.

The most commonly adopted material for electronic memory applications is $Ge_2Sb_2Te_5$ (GST) since it allows the best performance in terms of speed and scalability [5]. The GST exhibits a polymorphism in the crystalline phase. The stable structure, formed at temperatures above 250 °C, is trigonal, with space group (P-3m1), in which the Ge/Sb and Te planes form building blocks composed of one formula unit stacked along the hexagonal c axis [6,7]. This phase is usually obtained at the end of the manufacturing process of a memory cell. By rapid electric pulses, instead, a metastable phase with rock-salt structure (space group Fm-3m) is obtained, wherein Te atoms occupy the anions sublattice, while the cations sublattice is shared by Ge and Sb atoms and lattice vacancies [7]. In thin films, this phase is obtained at temperatures between 130 and 200 °C. Since the number of Te atoms exceeds the number of Ge and Sb atoms, there is a large amount (10%) of structural vacancies. In the metastable rock-salt phase, the vacancies are randomly distributed in the Ge/Sb sublattice. Instead, the trigonal phase is a layered structure built up by stacked atomic plane sequences of nine planes arranged along the hexagonal c axis [6,7]. According to the structure proposed by Matsunaga *et al.* [7] based on x-ray diffraction (XRD) analyses, the sequence of the layers in the trigonal phase is Te-Sb/Ge-Te-Ge/Sb-Te-Sb/Ge-Te, taking into account the presence of Ge/Sb intermixing in the cation layers. The two adjacent Te planes are weakly bound by van der Waals forces, giving rise to relatively large separations (van der Waals gaps) [8]. Structures with separated Ge and Sb planes have also been proposed by Petrov *et al.* (in which the Te atoms at the van der Waals gaps are bonded with Ge atoms only) [9] or Kooi and De Hosson (KH) [6] (with Te at the gap bonded with Sb atoms only). The latter corresponds to a structure in which two GeTe units are intercalated into the Sb_2Te_3 unit. According to first principles calculations, the KH sequence is slightly more stable at zero temperature. At finite temperatures, entropy effects are expected to lead to Ge/Sb intermixing.

Based on first principle calculations, Kim *et al.* [10–12] and Zhang *et al.* [13] predicted that trigonal GST in the sequence of Petrov *et al.* is a topological insulator (TI), while the KH sequence is not, but possesses interface states resembling the surface states of Sb_2Te_3 and can be regarded as a short-period superlattice of TI Sb_2Te_3 units and band insulator GeTe units, in which the electronic properties are determined by the Sb-Te-v-Te-Sb layers. In general, the TI properties are predicted to be very sensitive to the Te-v-Te distance, mainly determined

*Corresponding author: antonio.mio@imm.cnr.it

by the presence of van der Waals gaps, and are controlled by the degree of disorder, being completely destroyed when Ge migrates into the gaps [10,13].

Disorder not only has a large effect in determining the TI properties, but it also has an impact on the transport properties. Indeed, it has been experimentally observed that by annealing GeSbTe alloys at different temperatures, one can tune the degree of disorder and even induce an Anderson insulator-to-metal transition [14,15]. Recently, it has been shown that the ordering of the vacancies is the microscopic origin of this transition [16,17]. In particular, in the disordered rock-salt phase, obtained at low annealing temperature, the states at the Fermi energy are localized inside vacancy clusters. Thermal annealing at higher temperatures dissolves the clusters and orders the vacancies into planes, eventually leading to metallic behavior [16,17]. Vacancy disorder has a pronounced impact on the thermal transport as well, modulating the thermal conductivity of GeSbTe alloys [18].

Therefore the possibility to tune the disorder and to experimentally evidence its effect by structural measurements is very attractive for many applications, among them being the development of thermoelectric devices with high figure of merit and of temperature-independent resistors [19,20]. Also of interest is the possibility to develop conceptually new memory devices that combine the merits of phase-change memory, magnetic data storage, and quantum computing, thanks to the topological insulating properties [21], or to develop phase change memories based on the crystalline states, allowing the reduction of the RESET current [22].

In this paper, we study the stability of the crystalline phases and the evolution of the optical and electrical properties as a function of increasing disorder. Disorder is induced by ion irradiation characterized by diluted cascades, and its effects are studied by electrical and structural measurements. We find that disorder not only affects the electronic properties but is also crucial in determining the stability of the trigonal and cubic crystalline structures. The maximum degree of disorder that can be sustained by these structures is assessed both experimentally and theoretically.

II. METHODS

A. Sample preparation

$Ge_2Sb_2Te_5$ (GST) samples, 50 nm thick, have been deposited by dc sputtering at room temperature (RT) in the amorphous phase on thermally oxidized Si (100) wafers. The samples have been subsequently annealed at 200 °C or 350 °C in order to convert the material into the rock-salt or the trigonal stable phase, respectively. All the samples were polycrystalline and have been then irradiated using 150 keV Ar^+ ions at different fluences in the range from 1×10^{11} cm^2 to 5×10^{14} cm^{-2}. The projected range of Ar^+ ions, according to Stopping and Range of Ions in Matter SRIM software calculations, is 90 nm, larger than the GST layer thickness. Therefore, no Ar^+ ions stop into the GST film, and the energy loss, both nuclear and electronic, is quite uniform across the film thickness. The sputtering yield for Ge, Sb, and Te for Ar at 150 keV is about 0.3 atoms ion^{-1}. This means that for the maximum fluence (5×10^{14} cm^{-2}), less than one-tenth of a monolayer is sputtered; therefore, this effect is negligible.

The irradiation has been performed at RT and, for comparison, at 77 K. The beam current was kept constant and equal to 30 nA cm^{-2}.

B. Experimental details

A HeNe laser with wavelength 633 nm has been used as an optical probe for the *in situ* reflectivity measurements. The laser beam reflected by the sample is collected by a photodiode positioned outside the vacuum chamber.

After irradiation at different fluences, the electrical properties have been studied by measuring the sheet resistance with a four point probe, and its temperature dependence has been evaluated using a Temptronics thermal chuck, in the range from −20 °C to 30 °C in order to avoid possible annealing of the defects produced during the ion irradiation. For resistance measurements, a HP4156B parameter has been employed.

The structure of the sample after irradiation has been studied by XRD measurements in symmetric or grazing configuration with incident angle of 0.4°. A Bruker D8 Discover diffractometer has been employed. The x-ray wavelength is 1.54056 Å. The spectra have been acquired with a step size 0.02°, and the collection time was 15 sec step^{-1} or 30 sec step^{-1}. The lattice parameters were determined by cross-fitting the peaks positions with the corresponding lattice structure (as defined by the space group), with an uncertainty of ±0.001 nm.

Raman spectra have been collected by a Horiba Jobin Yvon HR800 system equipped with a 633 nm HeNe laser. In order to avoid heating of the sample, the power of the laser was kept below 1 mW, with a laser spot diameter of about 4 μm. The spectral window is 320 cm^{-1}, and the resolution is 0.2 cm^{-1}. Each spectrum has been acquired using three accumulations, each with collecting time of 40 s. Four different regions have been sampled.

Further analyses to determine the microstructure and the grain size have been conducted by transmission electron microscopy (TEM) using a JEOL 2010F operating at 200 keV and equipped with a low magnification camera for electron diffraction analyses. Samples were prepared at RT by mechanical polishing and chemical etching to avoid any artifact due to heating and/or milling, obtaining a membrane of 50 nm of capped GST on a thin layer of silicon oxide.

C. Simulation details

Density functional theory (DFT) simulations have been carried out with QUICKSTEP [23], a mixed Gaussian and plane-wave code, included in the CP2K package [24]. Kohn-Sham orbitals are expanded in a Gaussian-type basis set with triple-zeta plus polarization quality, whereas the charge density is expanded in plane waves, employing a cutoff of 300 Ry. Scalar-relativistic Goedecker-Teter-Hutter pseudopotentials [25] and gradient corrected functionals are used [26]. We do not include spin-orbit coupling, which is crucial to describing TI phases, but has negligible effect on the structural properties discussed in the following section. We also note that inclusion of spin-orbit coupling does not lead to any qualitative change in electron localization properties in strongly disordered models [27]. The Brillouin zone is sampled at the Γ point.

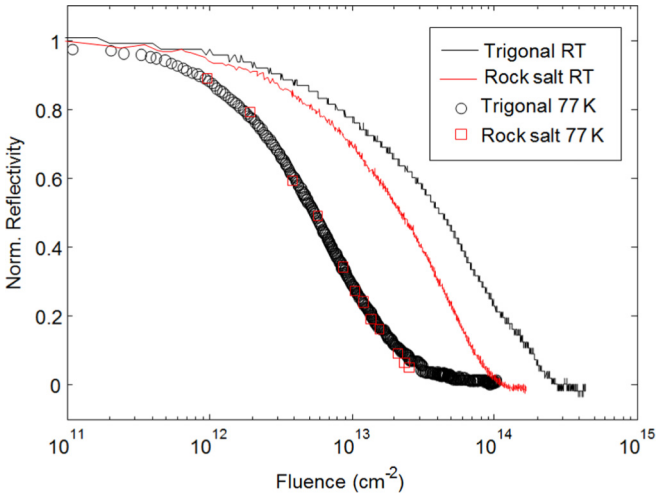

FIG. 1. Normalized reflectivity as a function of irradiation fluence at RT (lines) or 77 K (symbols).

III. RESULTS AND DISCUSSION

Figure 1 shows the normalized reflectivity as a function of the fluence, as measured during irradiation of the cubic or trigonal GST at RT or at 77 K. The reflectivity decreases as the fluence increases, down to a minimum value, corresponding to the complete amorphization [5]. Interestingly, a higher fluence is required at RT for the amorphization of the stable phase. The reflectivity versus fluence exhibits an exponential dependence, and by fitting the data we can evaluate the amorphization threshold, defined as the fluence required to decrease the reflectivity by a factor $1\,e^{-1}$. The obtained amorphization threshold for the rock-salt phase is $3 \times 10^{13}\,cm^{-2}$, while for the stable trigonal phase it is $8 \times 10^{13}\,cm^{-2}$. At low temperature, since the produced disorder cannot be recovered by thermal motion, all the displaced atoms practically remain in the disordered positions, and the material becomes amorphous at lower fluence, equal for the two structures. At RT, instead, thermal motion produces atomic rearrangement and disorder recovery [28]. Therefore some defects can be annihilated, and the atoms can reach more stable configurations. As we will show in the following, this effect determines the observed differences between the two crystalline structures.

Figure 2(a) shows the resistivity measured *ex situ* as a function of the fluence for irradiation at RT. In both the crystalline phases at fluences below $1 \times 10^{13}\,cm^{-2}$, no resistivity variation occurs. As the fluence increases, the resistivity increases also and reaches the value of 1000 Ω cm, typical of the amorphous phase. In agreement with the optical measurements, a higher fluence is required to reach the maximum resistivity in the case of the trigonal phase. The temperature dependence of the resistivity can be well described by measuring the slope of the resistivity as a function of temperature, i.e., the temperature coefficient of resistance (TCR). The results are shown in Fig. 2(b) as a function of the irradiation fluence. In the rock-salt phase the TCR is negative and continues to decrease as a function of the fluence. The trigonal phase is instead metallic (TCR > 0), but the TCR becomes negative after irradiation with a fluence of $2 \times 10^{13}\,cm^{-2}$ and then continuously decreases. The change of sign occurs at a resistivity value of 7.2 mΩ cm, higher than the value of 4 mΩ cm expected for the maximum metallic resistivity value, as calculated in Ref. [14].

Structural damage produced by ion irradiation has been also investigated by Raman spectroscopy. Figure 3(a) shows the spectrum of the rock-salt phase before irradiation, exhibiting a strong peak at $106\,cm^{-1}$ and a broad signal at about $158\,cm^{-1}$. As the fluence increases, a progressive decrease of the main peak ($106\,cm^{-1}$) and an increase of the vibrational contribution at $152\,cm^{-1}$, typical of the amorphous material, are observed [29,30]. The spectrum of the amorphous film after irradiation at the highest fluence is shown as a dashed line.

Figure 3(b) shows the Raman spectra obtained at different irradiation fluences for a sample prepared in the trigonal phase. Two peaks, at 106 and $172\,cm^{-1}$, characterize the spectrum before irradiation (blue solid line), in agreement with results previously reported in literature [30,31]. According to *ab initio* calculations, the Raman peaks of the trigonal phase in the range 90–120 cm^{-1} are due to E-type modes (vibrations in the basal ab plane), while the peaks above $150\,cm^{-1}$ are due to A-type phonons (vibrations along the stacking c axis) [32]. In particular, it is found that the A mode at highest frequency (A_{1g}) is modulated by the outermost Te-X bond, closer to Te-Te gaps [32]. This bond, according to the theoretical calculations, is strictly related to the TI properties. The intensity of the peak A_{1g} at $172\,cm^{-1}$ continuously decreases

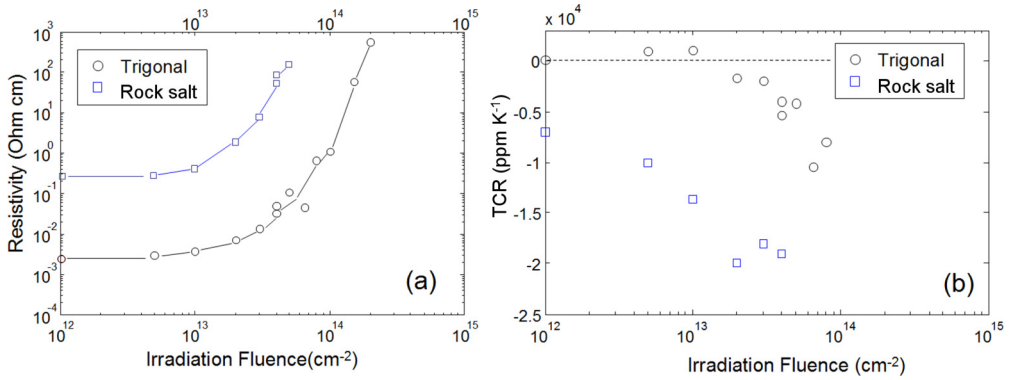

FIG. 2. (a) Resistivity and (b) temperature coefficient of resistance as a function of irradiation fluence for the rock-salt (squares) and the trigonal (circles) phase.

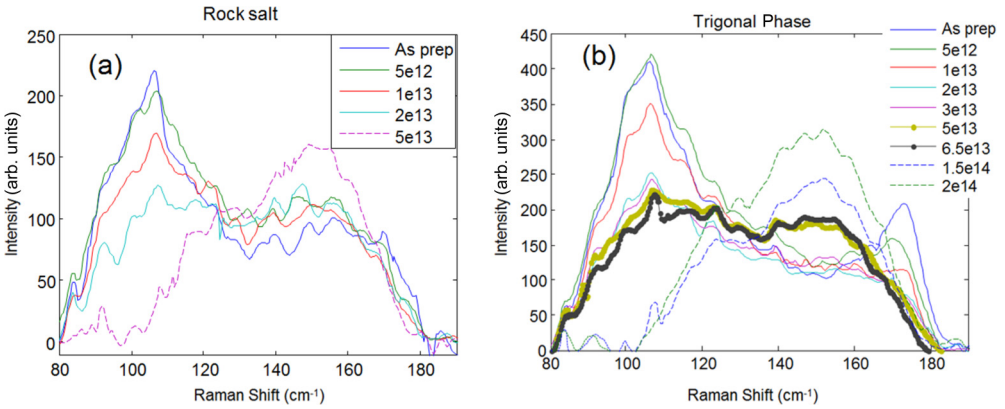

FIG. 3. Raman spectra acquired as a function of irradiation fluence for GST films prepared in the rock-salt (a) or in the trigonal stable phase (b).

as the irradiation fluence increases and completely disappears at a fluence of $2 \times 10^{13}\,\mathrm{cm}^{-2}$, while a Raman signal at about $155\,\mathrm{cm}^{-1}$ is detected, increasing with the fluence. A Raman signal in this region, ascribed to Ge-Te and Sb-Te bonds, is usually observed in amorphous (at $152\,\mathrm{cm}^{-1}$) and in cubic GST (at $160\,\mathrm{cm}^{-1}$). For fluences above the amorphization threshold ($8 \times 10^{13}\,\mathrm{cm}^{-2}$), the typical Raman spectrum of the amorphous phase is obtained (dashed lines).

The fluence of $2 \times 10^{13}\,\mathrm{cm}^{-2}$ is particularly interesting since at such value the intensity of the A_{1g} peak at $172\,\mathrm{cm}^{-1}$ disappears, and the TCR changes sign, as shown in Fig. 2(b). This observation establishes a clear link between the metallic conduction and a structural feature, indicating that the disorder produced by ion irradiation at low fluence first modifies the bond of Te atoms closer to the Van der Waals gaps; the loss of this peculiar feature is linked to the disappearance of the delocalized electronic states, which are responsible for the metallic conduction.

Above the fluence of $2 \times 10^{13}\,\mathrm{cm}^{-2}$ and below the amorphization threshold there is a transition regime, highlighted in Fig. 3(a) by plots with dots and lines, in which only a fraction of the film is amorphous. To determine the crystalline phase and the microstructure of the film, XRD and TEM analyses have been performed.

Figures 4(a) and 4(b) show, for the rock-salt phase and the trigonal phase, respectively, the XRD patterns acquired in grazing incidence configuration for the as-prepared film and for samples irradiated with a fluence of Ar^+ $2 \times 10^{13}\,\mathrm{cm}^{-2}$ or $4 \times 10^{13}\,\mathrm{cm}^{-2}$. For the metastable phase, the diffraction pattern of the as-prepared sample has the peaks expected for a rock-salt lattice. At a fluence of $2 \times 10^{13}\,\mathrm{cm}^{-2}$, the intensity of the diffraction peaks is reduced, indicating a lower degree of crystalline order due to a decrease in the coherent grain size, defects formation, and/or local amorphization. The lattice parameter slightly increases, changing from 0.596 nm to 0.597 nm, suggesting an expansion induced by the increase of the vacancy concentration produced by irradiation. The fluence of $4 \times 10^{13}\,\mathrm{cm}^{-2}$ is higher than the amorphization threshold, defined as reduction of the reflectivity to $1\,\mathrm{e}^{-1}$ of its initial value, and indeed, the spectrum shows a broad contribution, typical of the amorphous material and low intensity peaks produced by the fraction of material still in the crystalline rock-salt state.

For the GST trigonal sample, the lattice parameters measured before irradiation are $a = b = 0.420\,\mathrm{nm}$ and $c = 1.715\,\mathrm{nm}$. According to TEM analyses in cross section [17], the sample along the (001) direction is made by building blocks containing nine layers separated by van der Waals gaps in between two consecutive Te planes. Ge and Sb atoms are mixed in the cation layers, but the planes close to the Te atoms adjacent to the van der Waals gaps are rich in Sb (approaching the KH sequence). After irradiation with a fluence of Ar^+ $2 \times 10^{13}\,\mathrm{cm}^{-2}$, although the material mostly retains its crystalline structure, the peaks slightly shift towards

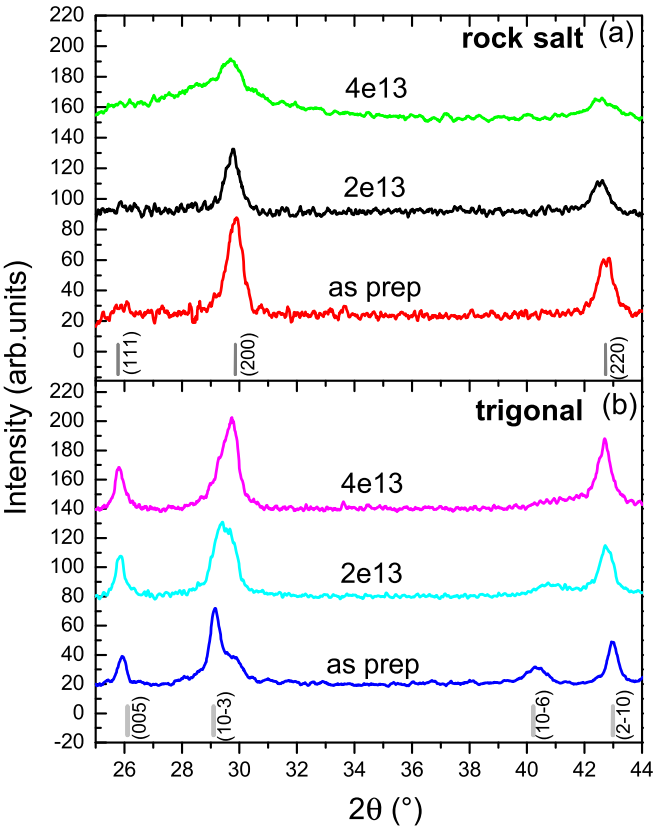

FIG. 4. The XRD patterns of the as-prepared crystalline films and after irradiation with a fluence of $2 \times 10^{13}\,\mathrm{cm}^{-2}$ or $4 \times 10^{13}\,\mathrm{cm}^{-2}$. (a) (b) The case of rock-salt and trigonal initial phase, respectively.

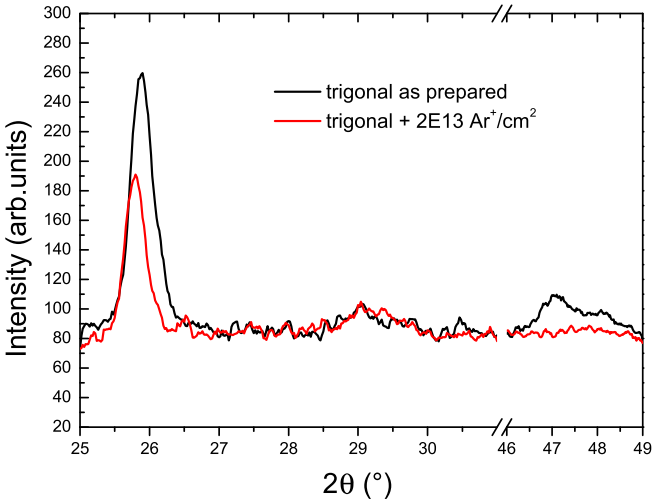

FIG. 5. Symmetric x-ray diffraction pattern of the trigonal phase as prepared and after irradiation at 2×10^{13} cm^{-2}.

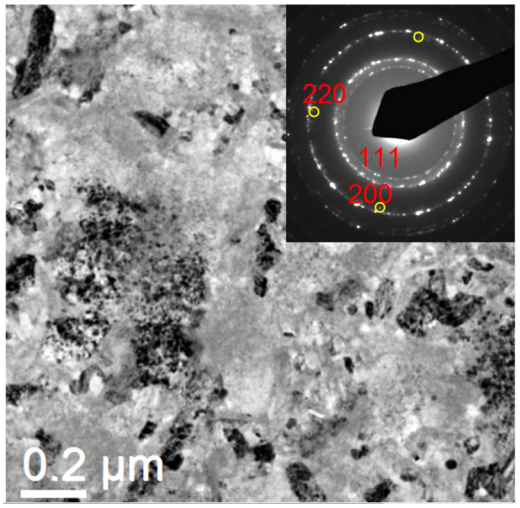

FIG. 6. Bright field TEM micrograph of a sample prepared with trigonal structure, after irradiation at 4×10^{13} cm^{-2} and (inset) selected area electron diffraction pattern. Red index indicate the rock-salt planes. Yellow circles are spots corresponding to the trigonal structure.

2θ values closer to those of the rock-salt structure. The samples were also analyzed in symmetric configuration (Bragg Brentano) to extract information on the crystallographic planes parallel to the surface. This analysis, reported in Fig. 5, shows a large texturing of the (001) planes in the trigonal as prepared film. After irradiation at a fluence of 2×10^{13} cm^{-2}, the film remains textured, as testified by the intense peak related to the (005) planes; nevertheless, it was observed that the (009) peak disappears. The disappearance of the (009) peak, combined with the persistence of the (005) peak, indicates that the material is mostly crystalline and textured, but the nine-plane periodicity is lost. This finding again addresses a link between the metallic conduction and the bond of Te atoms close to the Van der Waals gaps.

After irradiation at a fluence of 4×10^{13} cm^{-2}, the trigonal film is still crystalline, but all the diffraction peaks are shifted approaching the positions of the rock-salt phase and the (10-6) peak disappears. Confirming this observation, the TEM micrograph of Fig. 6, acquired for the same sample and irradiated at a fluence of 4×10^{13} cm^{-2}, shows the presence of small crystalline grains, with size 3–5 nm, embedded into large grains. From the analysis of selected area diffraction, shown in the inset, we found that the diffraction rings correspond to the electron diffraction pattern of the rock-salt phase (indexed in red) and are produced by the small randomly oriented crystalline grains, according to what was found by XRD. On the other hand, the spots highlighted by the yellow circles are the diffraction spots of a single grain with the trigonal structure.

Damage accumulation with increasing ion fluence up to amorphization is a well-known phenomenon that has been extensively studied in both elemental and compound crystals [33]. However, the different behavior shown by the two GST crystalline phases during ion irradiation at RT is quite unusual. For the same chemical composition, indeed radiation damage is usually independent of the target structure. Ion trajectories and related effects, such as displacement rate, should not depend, from a purely ballistic point of view, on the material crystalline structures, apart from directional effects, such as planar or axial channeling, which should be avoided. These are clearly not relevant to the present study, as confirmed by the data shown in Fig. 1 for the low temperature irradiation. The different behavior observed at RT is then related to the mobility of the displaced target atoms.

According to the trigonal structure proposed by Matsunaga *et al.* [7] and calculated by Da Silva *et al.* [34] for $Ge_2Sb_2Te_5$, in the cationic planes perpendicular to the c direction, Ge and Sb atoms are mixed. Therefore, disorder produced in the ab planes is not expected to largely modify the structure. Moreover, phase change alloys are characterized by a very high atomic mobility, and the collision cascade in the present experiment is quite dilute, i.e., a direct recombination of vacancy and interstitials is prevented. It is therefore plausible to assume that the atoms displaced by the impinging ions diffuse and that stop in the van der Waals gaps act as preferential sinks. Indeed, Raman analyses have shown that for very low irradiation fluences in the trigonal structure, the major effect is produced in the Te-X bonds of Te atoms closer to the Van der Waals gaps. The disappearance of the characteristic peak of the trigonal phase in the spectrum, at 172 cm^{-1}, is accompanied by the disappearance of the diffraction peak of the (009) planes and by the change of sign in the TCR, suggesting the disappearance of the delocalized electronic states, responsible for the metallic conduction, and the formation of more localized states. Such a metal-insulator transition is clearly driven by disorder.

By employing the SRIM code for the evaluation of the displacements of atoms (DPA) produced by the ion irradiation, we can also have an estimation of the degree of disorder required to produce the observed phase transitions. At a fluence of 2×10^{13} cm^{-2}, the total DPA is 9%. Among these, 4.6% is due to the displacement of Ge and Sb atoms. The van der Waals gaps can be considered as planes with vacancy occupation of 100%. Assuming that about half of the total of displaced atoms are trapped in the gaps, the vacancy occupancy is reduced to

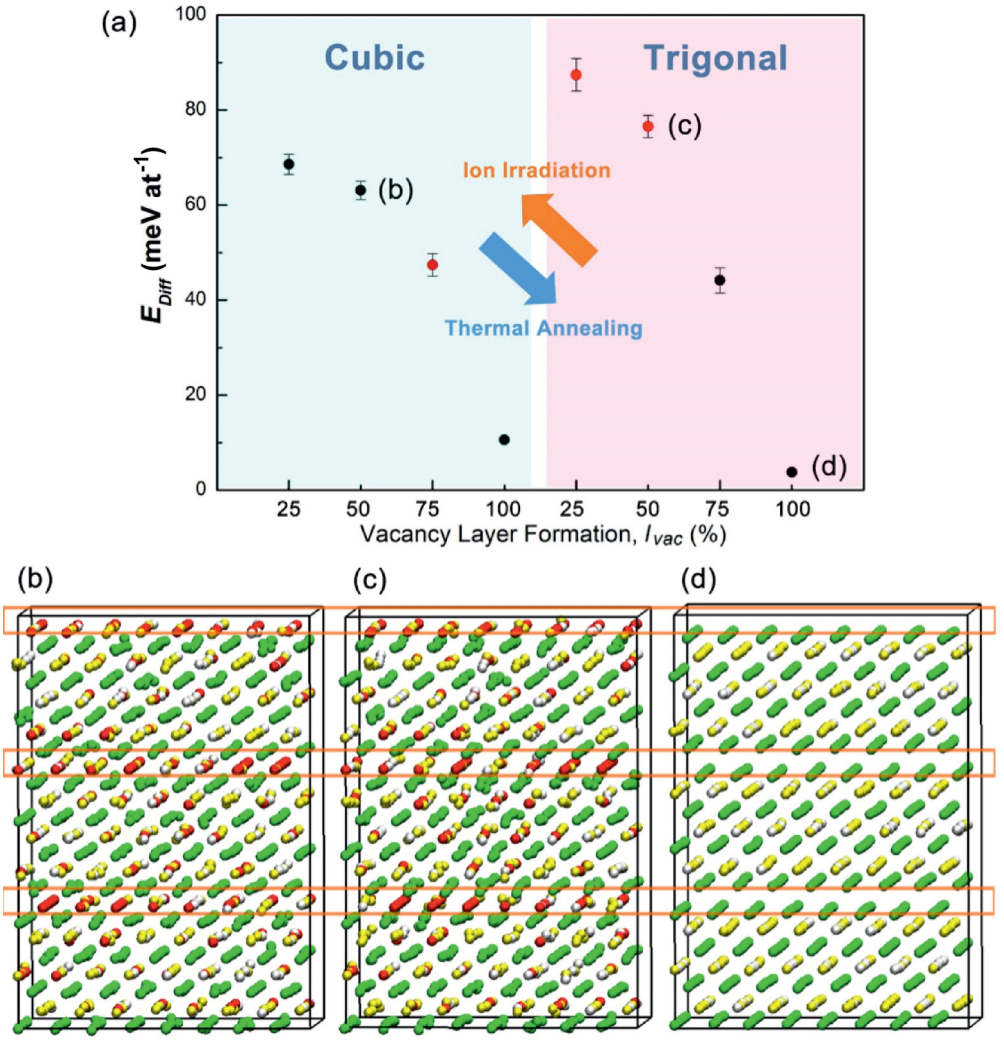

FIG. 7. (a) Energy plot of disordered cubic and trigonal $Ge_1Sb_2Te_4$ with different percentage of vacancy layer formation, l_{vac}. For each model, we average over four geometry configurations. Red points are the configurations that are less likely to be observed experimentally because they are energetically less favorable than their (cubic or trigonal) counterparts. (b)–(d) The relaxed structures of Cub-50%, Tri-50%, and Tri-100%. Ge, Sb, and Te atoms are rendered with gray, yellow, and green spheres. Atomic vacancies are highlighted with red spheres. The depleted layers and van der Waals gaps are marked with orange boxes.

60%. Considering the high activation energy for migration of Te atoms and the unfavorable Te-Te antibonds [35], the probability to find displaced Te atoms inside the gaps is very low, and we can consider only Ge and Sb atoms.

This process can be regarded as a vacancy disordering process, inducing a transition from metallic to insulating phase, which is opposite to the vacancy ordering process upon thermal annealing that drives the insulator-to-metal transition investigated in Refs. [14–17] and [35]. In a previous DFT work [16], the cubic-to-trigonal structural transition, as well as the insulator-to-metal transition driven by ordering upon thermal annealing, has been investigated in crystalline $Ge_1Sb_2Te_4$. It has been shown that the crystal structure with trigonal stacking becomes lower in energy than the cubic one when depleted layers are formed with vacancy concentrations around 75%. This is in line with our current experimental findings. Here, we carry out further DFT simulations of disordered $Ge_1Sb_2Te_4$ with trigonal stacking corresponding to partial (50% and 25%) formation of vacancy layers, denoted as Tri-50% and Tri-25%. The same model size as in Ref. [16] is considered (1008 atoms) to enable a fair comparison. For each model, we average over four independent geometry configurations. Upon structural optimization, all the trigonal models exhibit metastable configurations characterized by small atomic distortions, and the total energies of Tri-50% and Tri-25% are ~ 13 and 19 meV atom^{-1} higher than those of the corresponding cubic models, Cub-50% and Cub-25% [see Fig. 7(a)]. The relaxed structures of the disordered Cub-50%, disordered Tri-50% and ordered Tri-100% are shown in Figs. 7(b)–7(d). We also study the $Ge_2Sb_2Te_5$ case, and the trends turn out to be the same, e.g., Tri-50% is ~ 15 meV atom^{-1} higher in energy than Cub-50%.

The high energy penalty provides the driving force for the structural transition from trigonal to cubic stacking upon ion irradiation, as observed in our XRD and TEM experiments (Figs. 4 and 6) for the as-prepared trigonal $Ge_2Sb_2Te_5$, ion irradiated at RT. In these samples, for a total DPA of 9–15%, corresponding to a vacancy occupancy of less than 50%, the material becomes very similar to the rock-salt

structure. At even higher irradiation fluences, the material becomes amorphous (24% DPA), indicating that the bonds are completely changed. Moreover, for a fluence of 1×10^{13} cm^{-2} corresponding to a vacancy occupation of 80%, a small Raman peak at 172 cm^{-1} is still detectable, and a metallic dependence of the resistivity is measured, while for a fluence of 2×10^{13} cm^{-2}, the sample displays a negative TCR (see Fig. 2 and Fig. 4). These findings indicate that the metal-insulator transition and the structural transition are not correlated, in agreement with previous works [14,16].

IV. CONCLUSION

We have studied the effect of disorder induced by ion irradiation on the structural and the electrical properties of polycrystalline GST thin films. In the rock-salt structure, the increasing disorder produces progressive amorphization. In the trigonal phase, instead, several transitions are observed, triggered by a vacancy disordering process produced by the ion irradiation. First, the electronic transition from metallic to insulating behavior is accompanied by the disappearance of the Raman peak at 172 cm^{-1}, linked to the bonds of Te atoms close to the van der Waals gaps. Then, by further increasing the disorder, the crystalline structure becomes close to the metastable rock-salt phase, with the appearance of small grains with cubic structure within the large trigonal grains. The high energy penalty of vacancy disorder in the trigonal phase provides the driving force for the inverse trigonal to cubic structural transition, as evidenced by the DFT simulations. The observed phase evolution underlines the role of the van der Waals gaps in determining the electrical properties of GeSbTe phase change materials and the stability of the trigonal structure.

ACKNOWLEDGMENTS

The authors would like to acknowledge Prof. Matthias Wuttig for the inspiring and fruitful discussions. We also acknowledge S. Tatì for his technical assistance during ion irradiation experiments. W.Z. and R.M. acknowledge the computational resources provided by the HPCC platform of Xi'an Jiaotong University and by JARA-HPC from RWTH Aachen University under Project No. JARA0089. W.Z. gratefully thanks the Young Talent Support Plan of Xi'an Jiaotong University. R.M. acknowledges funding by the Deutsche Forschungsgemeinschaft (DFG) within the collaborative research center Project No. SFB 917 "Nanoswitches".

[1] S. R. Ovshinsky, Phys. Rev. Lett. **21**, 1450 (1968).
[2] G. W. Burr, M. J. Breitwisch, M. Franceschini, D. Garetto, K. Gopalakrishnan, B. Jackson, B. Kurdi, C. Lam, L.A. Lasras, A. Padilla, B. Rajendran, S. Raoux, and R. S. Shenoy, J. Vac. Sci. Technol. B **28**, 223 (2010).
[3] S. Lai and T. Lowrey, IEDM Technical Digest: International Electron Devices Meeting, Dec 2–5, Washington, DC, USA (2001), pp. 36.5.1–36.5.4.
[4] A. Redaelli and A. Pirovano, Nanotechnology **22**, 254021 (2011).
[5] N. Yamada, E. Ohno, K. Nishiuchi, N. Akahira, and M. Takao, J. Appl. Phys. **69**, 2849 (1991).
[6] B. J. Kooi and J. Th. M. De Hosson, J. Appl. Phys. **92**, 3584 (2002).
[7] T. Matsunaga, N. Yamada, and Y. Kubota, Acta Crystallogr. Sect. B **60**, 685 (2004).
[8] R. H. S. Winterton, Contemp. Phys. **11**, 559 (1970).
[9] I. I. Petrov, R. M. Imamov, and Z. G. Pinsker, Sov. Phys. Crystallogr. **13**, 339 (1968).
[10] J. Kim, J. Kim, and S.-H. Jhi, Phys. Rev. B **82**, 201312(R) (2010).
[11] J. Kim, J. Kim, K.-S. Kim, and S.-H. Jhi, Phys. Rev. Lett. **109**, 146601 (2012).
[12] J. Kim and S.-H. Jhi, J. Appl. Phys. **117**, 195701 (2015).
[13] H. Zhang, C.-X. Liu, X.-L. Qi, X. Dai, Z. Fang, and S.-C. Zhang, Nat. Phys. **5**, 438 (2009).
[14] T. Siegrist, P. Jost, H. Volker, M. Woda, P. Merkelbach, C. Schlockermann, and M. Wuttig. Nat. Mater. **10**, 202 (2011).
[15] N. P. Breznay, H. Volker, A. Palevski, R. Mazzarello, A. Kapitulnik, and M. Wuttig, Phys. Rev. B **86**, 205302 (2012).
[16] W. Zhang, A. Thiess, P. Zalden, R. Zeller, P. H. Dederichs, J.-Y. Raty, M. Wuttig, S. Blügel, and R. Mazzarello, Nat. Mater. **11**, 952 (2012).
[17] V. Bragaglia, F. Arciprete, W. Zhang, A. M. Mio, E. Zallo, K. Perumal, A. Giussani, S. Cecchi, J. Boschker, H. Riechert, S. Privitera, E. Rimini, R. Mazzarello, and R. Calarco, Sci. Rep. **6**, 23843 (2016).
[18] K. S. Siegert, F. R. L. Lange, E. R. Sittner, H. Volker, C. Schlockermann, T. Siegrist, and M. Wuttig, Rep. Prog. Phys. **78**, 013001 (2015).
[19] M. Kumar, A. Vora-ud, T. Seetawan, and J. G. Han, Energy Technol. **4**, 375 (2016).
[20] S. Privitera, G. D'Arrigo, A. M. Mio, N. Piluso, F. L. Via, and E. Rimini, IEEE Trans. Electron Devices **61**, 2879 (2014).
[21] J. E. Moore, Nature (London) **464**, 194 (2010).
[22] R. Simpson, P. Fons, A. V. Kolobov, T. Fukaya, M. Krbal, T. Yagi, and J. Tominaga, Nat. Nanotech. **6**, 501 (2011).
[23] J. VandeVondele, M. Krack, F. Mohamed, M. Parrinello, T. Chassaing, and J. Hutter, Comput. Phys. Commun. **167**, 103 (2005).
[24] J. Hutter, M. Iannuzzi, F. Schiffmann, and J. VandeVondele, WIREs Comput. Mol. Sci. **4**, 15 (2014).
[25] S. Goedecker, M. Teter, and J. Hutter, Phys. Rev. B **54**, 1703 (1996).
[26] J. P. Perdew, K. Burke, and M. Ernzerhof, Phys. Rev. Lett. **77**, 3865 (1996).
[27] W. Zhang, M. Wuttig, and R. Mazzarello, Sci. Rep. **5**, 13496 (2015).
[28] P. J. Schultz, C. Jagadish, M. C. Ridgway, R. G. Elliman, and J. S. Williams, Phys. Rev. B **44**, 9118(R) (1991)
[29] P. Nemec, V. Nazabal, A. Moreac, J. Gutwirth, L. Bene, and M. Frumar, Mater. Chem. Phys. **136**, 935 (2012).
[30] K. S. Andrikopoulos, S. N. Yannopoulos, A. V. Kolobov, P. Fons, and J. Tominaga, J. Phys. Chem. Solids **68**, 1074 (2007).

[31] R. De Bastiani, E. Carria, S. Gibilisco, A. Mio, C. Bongiorno, F. Piccinelli, M. Bettinelli, A. R. Pennisi, M. G. Grimaldi, and E. Rimini, J. Appl. Phys. **107**, 113521 (2010).

[32] G. C. Sosso, S. Caravati, C. Gatti, S. Assoni, and M. Bernasconi, J. Phys.: Condens. Matter **21**, 245401 (2009).

[33] M. Nastasi and J. W. Mayer, *Ion Implantation and Synthesis of Materials* (Springer-Verlag, Berlin, 2006).

[34] J. L. F. Da Silva, A. Walsh, and H. Lee, Phys. Rev. B **78**, 224111 (2008).

[35] B. Zhang, W. Zhang, Z.-J. Shen, Y.-J. Chen, J.-X. Li, S.-B. Zhang, Z. Zhang, M. Wuttig, R. Mazzarello, E. Ma, and X.-D. Han, Appl. Phys. Lett. **108**, 191902 (2016).